Preprint
UCRL-JC-141320

Matrix-Dominated Performance of Thick-Section Fiber Composites for Flywheel Applications

S. J. DeTeresa, L. M. Allison, D. C. Freeman, S. E. Groves

This article was submitted to
Society for the Advancement of Material and Process Engineering
2001 Symposium, Long Beach, CA., May 5-10, 2001

U.S. Department of Energy
Lawrence Livermore National Laboratory

January 17, 2001

This work was performed under the auspices of the United States Department of Energy by the University of California, Lawrence Livermore National Laboratory under contract No. W-7405-Eng-48.

MATRIX-DOMINATED PERFORMANCE OF THICK-SECTION FIBER COMPOSITES FOR FLYWHEEL APPLICATIONS

S. J. DeTeresa, L. M. Allison, D. C. Freeman, and S. E. Groves
University of California
Lawrence Livermore National Laboratory
Livermore, CA 94550

ABSTRACT

An Achilles heel for the performance of thick-section, cylindrical fiber composite flywheels is the poor interlaminar properties of the material. Methods that have been used to minimize or eliminate radial tensile stresses include prestressing concentric cylinders and mass loading. There can also be significant interlaminar shear stresses at the edges of mass-loaded flywheels and in flywheels for high-power density applications where abrupt braking results in high torque levels. To specify adequate safety factors for thick-section flywheels used in these applications, the failure envelope and fatigue behavior under combined interlaminar stresses are required. Using a hollow cylindrical specimen, which was subjected to combined axial compression and torsion, results for fatigue and failure were generated for several flywheel material systems. Interlaminar compression resulted in significant enhancements to the interlaminar shear strength and results were compared to the predictions of proposed three-dimensional composite failure models. The interlaminar shear fatigue behavior of a carbon/epoxy system was also studied and compression was found to greatly enhance fatigue life. The results demonstrate that radial compression stresses can yield improvements in the interlaminar shear strength and fatigue lifetimes of composite flywheel rotors.

KEYWORDS: Applications-Flywheel, Failure Criteria/Mechanisms, Fatigue

1. INTRODUCTION

In order to realize fully the potential of fiber composites in flywheels for high-energy and high-power density applications, rotors must be made with appreciable thickness. In most practical applications the construction of the rotor is by filament winding or lamination where the fiber is oriented in the $z\theta$ plane. Consequently, the performance of these rotors is limited by the weaker, matrix-dominated, radial strength rather than the fiber-direction strength of the composite. Due to the uncertainty in the ability of the composite rotor to withstand radial tensile stresses in long-term applications, many different approaches have been proposed and utilized to minimize or completely eliminate this stress. Some of these solutions involve the use of different materials to provide a reduction in radial tensile stress. One example is a rotor having a gradient in specific modulus (modulus/density) from a low value at the inner diameter to higher values at the outer diameter (1). During rotation, the softer, denser inner part of the rotor expands against the outer region and causes a reduction in radial tension stress. Another material solution is a thick-walled rotor made from concentric cylinders that are separated by a compliant material (2).

This work was performed under the auspices of the U. S. Department of Energy by the Lawrence Livermore National Laboratory under contract No. W-7405-Eng-48

Although these material solutions have been used with some success, they do not provide sufficient mitigation of the radial tensile stress for thick-walled composite rotors. In these cases, designers have resorted to structural solutions such as mass-loading the inner diameter of the rotor or building in residual compressive radial stresses during manufacture of the rotor. Although some level of residual stress can be generated by varying the tension in the fiber during filament winding (3), the magnitude of this stress is limited to only small values by the maximum tension that can be applied to the fiber without breaking it during rotor manufacture. Substantially higher values of residual radial compression are achieved by either press fitting relatively thin-wall concentric cylinders or bonding concentric cylinders with an adhesive that is pressurized during cure. In these cases where high levels of radial compression stress are generated (either by mass-loading or the combination of concentric cylinders), multidirectional laminates are used to minimize the chances of failure due to through-thickness (radial) compression. Furthermore, in the case of the mass-loaded rotors, there are significant interlaminar shear stresses at the ends of the rotor due to free-edge effects. For high-power density applications such as the power source for electric armaments, the quick discharge of energy results in an abrupt reduction in angular velocity and this "braking" can subject thick-walled rotors to high interlaminar shear stresses.

Successful design of thick-wall rotors that utilize the aforementioned approaches to radial tensile stress elimination requires some understanding of material failure and fatigue under combined interlaminar shear and compression stresses. While the failure due to combined in-plane stresses in fiber composite laminates has been well studied, little information is available concerning interlaminar failure under combined out-of-plane stresses. Since interlaminar strengths are dominated by matrix properties, it is expected that interactive stress effects exist for these delamination failure modes. Past experience has shown that benefits in interlaminar shear performance of joints can be obtained if there is some mechanism for providing through-thickness compression (4). Methods that have been developed to provide the enhanced compression include clamping action via bolts and self-generated compression in conical joints for composite cylinders (5).

There have been several studies to characterize the failure of glass fiber composites at cryogenic temperatures for application to insulation in the toroidal field coils of the International Thermonuclear Experimental Reactor (ITER) (6) and the Compact Ignition Tokamak (CIT) (7). In the latter, the strength of laminates tested at several orientations provided a fixed ratio of combined compression and shear, whereas in the former, compression was applied independently in a biaxial test device. However, due to the nature of the test design, interlaminar failure could only be attained under high compression levels. Although both studies revealed an increase in shear strength with compression, neither provided any measure of the deformation behavior in the combined stress state.

Study of fatigue under combined interlaminar shear and compression was also undertaken for the ITER project (6). This appears to be the only reported study of fatigue of fiber composites under combined interlaminar stresses.

In the present study, failure due to combined through-thickness compression and interlaminar shear was examined under quasi-static and fatigue loading conditions. Experimental results for several composite materials are presented and compared with the predictions of a few representative and well-known composite failure theories for three-dimensional stress states.

2. EXPERIMENTAL

The specimen developed for studies of fatigue and failure under combined interlaminar shear and compression is shown in Figure 1. Thick-section composites were machined into small "dogbone" samples having a hollow cylinder gage section and square ends for applying torque. A similar specimen had been used in the past to study individually the interlaminar shear and tensile strengths of fiberglass laminates (8). The present work extends the use of this specimen to study combined stress effects. The gage section of the specimens was machined using a high-speed diamond-grinding tool under flood coolant to nominal dimensions of 0.635 cm gage length, 1.59 cm inner and 2.10 cm outer diameters. The transition from square ends to the cylindrical gage section was made with a 0.635 cm radius. The 1.59 cm diameter holes were machined using a carbide drill and these holes served as the datum for grinding the outside contour and for aligning the specimens in test fixtures.

The specimen is not quite a thin-walled cylinder and in order to calculate maximum shear stresses from measured torque values, the following well-known equations for both purely elastic and plastic behavior were used:

$$\tau_e = \frac{2T}{\pi r_o^3\left(1 - r_i^4/r_o^4\right)} \qquad [1]$$

$$\tau_p = \frac{3T}{2\pi\left(r_o^3 - r_i^3\right)} \qquad [2]$$

where r_i and r_o are the inner and outer radii, respectively and T is the torque. Torque-twist curves were examined to determine if the behavior at failure was predominantly elastic or plastic and the corresponding equation was used to calculate the shear stress at failure. For this specimen, the maximum error in using either [1] or [2] is only 12%.

All tests were performed using MTS servohydraulic, biaxial test machines capable of controlling torque, rotation, normal force, and displacement. For static strength and fatigue tests, a constant compression force was applied while the specimen was twisted to failure under torque control. For elevated temperature tests, special water-cooled adapter fixtures were built to allow heating using a quartz clamshell oven while maintaining precise concentric and parallel alignment to the specimens. In the fatigue and elevated temperature tests, temperature was monitored using a thermocouple mounted directly to the specimen. Preliminary fatigue tests conducted using 3 and 30 Hz sawtooth waves showed that there were no heating effects at the higher rate and that the lifetimes were identical at the two frequencies. The slower rate was used for the higher stress fatigue tests to allow sufficient time for the test system to establish torque control. The lower stress, high-cycle tests were run at 30 Hz and were stopped prior to failure if the specimen survived 10^6 cycles. All fatigue tests were conducted at a shear stress ratio of R = 0.1.

Four different types of specimens were tested: a $[45/0/-45/90]_{XS}$ laminate of T300 carbon fiber with Hexcel F584 epoxy matrix, a $[0/90]_{XS}$ laminate of IM7 carbon fiber with Hexcel 8551-7 epoxy matrix, a liquid-molded E-glass, plain-weave fabric/vinyl ester laminate, and a filament-wound, $[90_2/\pm45]_{XS}$ panel of S2-glass/epoxy. All were machined from panels that were nominally 2.54 cm thick.

3. RESULTS

3.1 Failure Under Combined Interlaminar Stress The shear stress-strain response, as indicated by torque-twist curves, showed both enhanced strength and ductility under constant compression stress. Results for tests conducted at room temperature for all materials are shown in Figs. 2–5. The T300/F584, E-glass/vinyl ester, and S2-glass/epoxy laminates appear to be elastic to failure under pure interlaminar shear. However, under nearly all compression stresses, including relatively low values, the response becomes plastic. The increase in strength and ductility continued until compression levels approached the through-thickness compression strength. Cross-ply and quasi-isotropic laminates exhibit high interlaminar compression strengths, thereby allowing significant enhancement of the shear strength through large superimposed compression stresses.

The envelope for shear failure as a function of interlaminar compression for all materials is shown in Figure 6. The failure curves indicate that for the increase in shear strength up to the maximum value, the behavior is quadratic. The maximum shear strength enhancement was significant and varied from 55% for the E-glass fabric composite to 340% for the laminated T300/F584 composite.

3.2 Comparison with Three-Dimensional Failure Theories The biaxial strength results were compared with the predictions of representative three-dimensional failure theories for fiber composites. All of the theories examined were derived for failure at the ply level and stresses were calculated for the plies in the following manner. It was assumed that effects due to edge stresses could be ignored and that the through-thickness compression stress was uniform throughout the gage section. In order to calculate ply-level stresses, lamina elastic constants are needed to determine laminate elastic constants using a homogenization approach. There is a complete set of reported elastic constants, strength values, and interaction parameters for the IM7/8551-7 system (9). The laminate constants were calculated using the method proposed by Sun and Li (10). Laminate strains were then determined by applying interlaminar shear and compression stresses. These were used to determine ply-level stresses using the standard tensor transformation rules and lamina constitutive relations. For both cross-ply and quasi-isotropic laminates, the in-plane, ply-level stresses caused by through-thickness compression are identical and are of the form

$$\sigma_1 = -a\sigma,\ \sigma_2 = a\sigma,\ \sigma_3 = \sigma \qquad [3]$$

where σ_3 is the through-thickness stress, σ_1 is the fiber-direction (longitudinal) ply stress, σ_2 is the transverse ply stress, and a is a constant. Due to the cylindrical geometry of the specimens used in this study, the ply-level shear stress is a combination of longitudinal shear, σ_6, and transverse shear, σ_4. When the stress state given by [3] is considered in all the failure theories, it is found that the effect on both of these shear stresses is identical. Thus it is not necessary to determine if failure of the specimens is due to either type of shearing stress for the purposes of failure theory comparison.

The failure theories used to compare with the experimental results were the Tsai-Wu tensor polynomial theory (11), Hashin's theory (12) and Christensen's stress-based theory (13). The tensor polynomial is a single expression of all stresses and does not specific the type of failure. For the combination of stresses [3] and interlaminar shear, the condition for failure is

$$\sigma^2\left[a^2F_{11} + (a^2+1)F_{22} + 2a(1-a)F_{12} - 2aF_{23}\right] + \sigma\left[-aF_1 + (1+a)F_2\right] + F_{66}\sigma_6^2 = 1 \qquad [4]$$

where the failure parameters, F_i and F_{ii} are defined by

$$F_1 = \frac{1}{X_T} - \frac{1}{X_C},\ F_2 = \frac{1}{Y_T} - \frac{1}{Y_C}$$
$$F_{11} = \frac{1}{X_T X_C},\ F_{22} = \frac{1}{Y_T Y_C},\ F_{66} = \frac{1}{S_L^2} \qquad [5]$$

The remaining parameters, F_{12} and F_{23}, are interactive parameters that must be determined from multiaxial tests and values for the IM7/8551-7 system have been reported (9). The lamina strengths used to define the parameters [3] are

$$\begin{aligned} X_T &= \textit{longitudinal tensile strength} \\ X_C &= \textit{longitudinal compression strength} \\ Y_T &= \textit{transverse tensile strength} \\ Y_T &= \textit{transverse compression strength} \\ S_L &= \textit{longitudinal shear strength} \end{aligned} \qquad [6]$$

Only the magnitudes of the lamina strengths are used in the failure relations.

The Hashin and Christensen failure theories specify separate conditions for matrix- and fiber dominated failure. For the case of combined interlaminar shear and compression where $\sigma_2 + \sigma_3 < 0$ and the normal stresses are given by [3], the Hashin failure relation is

$$\frac{1}{Y_T}\left[\left(\frac{Y_T}{S_T}\right)^2 - 1\right]\sigma(1+a) + \frac{\sigma^2}{S_T^2}\left[\frac{(1+a)^2}{4} - a\right] + \frac{\sigma_6^2}{S_L^2} = 1 \qquad [7]$$

For the same stress state, the Christensen theory for matrix-dominated failure gives the condition

$$\alpha_1 k_1 \sigma(1+a) + (1+2\alpha_1)\left[\frac{1}{4}\sigma^2(a-1)^2\right] + \beta_1\sigma_6^2 = k_1^2$$
$$\alpha_1 = \frac{1}{2}\left(\frac{Y_C}{Y_T} - 1\right),\ k_1 = \frac{Y_C}{2},\ \beta_1 = \left(\frac{Y_C}{2S_L}\right)^2 \qquad [8]$$

The Hashin theory requires a value for the transverse shear strength, S_T, but this property is notoriously difficult to measure. It was decided to use a calculated value for S_T, which is a natural result of the Christensen theory. This estimate for S_T is

$$S_T = \frac{\sqrt{Y_T Y_C}}{2} \qquad [9]$$

The lamina elastic constants and strengths for the IM7/8551-7 system are summarized in Table 1. The interactive parameter F_{12} in the tensor polynomial theory [4] is taken to have a value of 8.4120E-07 MPa^{-2} as reported in reference (9). Also following (9), three values for the parameter F_{23} were examined: 1.2972E-05, 3.9139E-05, and –3.9139E-05

MPa^{-2}.

Using relations [4], [7], and [8] with vanishing shear stress provides predictions for failure under through-thickness compression alone. For the lamina constants given in Table 1, it is found that the parameter, a, that governs the magnitude of the two in-plane stresses is 0.435. Thus the ply-level longitudinal tensile stress and in-plane transverse compression stress are nearly half the magnitude of the applied through-thickness compression stress. The predictions for failure of cross-ply or quasi-isotropic laminates of IM7/8551-7 under interlaminar compression are summarized in Table 2. The three results for Tsai-Wu correspond to the three values of the parameter F_{23}. Comparison of these predictions with the failure envelope in Fig. 7 shows that almost all the theories predict failure at compression stresses less than those actually attained in the combined stress tests. Only Hashin theory appears to predict the observed high compression strength of the laminate.

Predicted failure envelopes for the combined stress of interlaminar shear and compression are shown in Fig. 7. In this figure, all data and predicted values have been normalized to the shear strength, S_L. All theories correctly predict the trend of increasing shear strength with pressure, but none actually capture the full extent of the experimentally observed strength enhancement. Regardless of which particular interaction parameter F_{23} is used in the tensor polynomial theory, the predictions agree with data over only a very limited range. Both the Christensen and Hashin theories do a somewhat better job of capturing the experimental results at low compression levels but depart significantly from these results when the compression stress is greater than four times the shear strength.

3.3 Fatigue Under Combined Interlaminar Stress Most of the shear fatigue studies were conducted to support development of composite flywheel rotors for electric armaments. In this environment, thick-walled rotors are subjected to residual radial compression from manufacture combined with interlaminar shear from "braking" during energy discharge. Additionally electrical self-heating results in a rotor steady-state temperature of 93°C. Results for interlaminar shear fatigue of IM7/8551-7 at temperature under different interlaminar compression levels are summarized in Figure 8. The open symbols with arrows denote tests that were halted after reaching 10^6cycles, which is defined as the run-out stress. These data show the increase in static strength (stress at N=1) with compression stress, which is similar to the enhancement seen at room temperature. The fatigue lifetime curves under 0 and 52 MPa compression are very similar in form. Both achieve a run-out condition at 75% of their respective static strengths. Furthermore, run-out under 52 MPa compression is attained at a shear stress that is greater than the uniaxial shear strength of the composite. Surprising results were obtained for fatigue tests under 103 MPa compression. No fatigue failure was observed up to shear stress levels of 96% of the static failure stress! The dotted line in Fig. 8 signifies that all specimens tested achieved run-out under shear fatigue load. Thus with only a moderate amount of compression, the mechanism for interlaminar shear fatigue failure was essentially eliminated. Although the precise nature of the fatigue damage mechanism is unknown, the improvement in life is likely related to the enhancement in interlaminar shear ductility with superimposed compression.

3. CONCLUSIONS

A study of the failure and fatigue of composites under combined interlaminar stresses was made to support design and development of thick-wall flywheel rotors. Compression was found to significantly enhance shear strength and ductility in four different composite material systems. Experimental results for IM7/8551-7 compared favorably with predictions of Hashin and Christensen three-dimensional failure models, but only up to moderate levels of compression stress. At higher stress levels, predicted strengths were

significantly lower than actually measured. A tensor polynomial theory severely underpredicted the increase in shear strength under compression. The use of different interactive failure parameters in applying this theory had little effect in improving the agreement with the experimental results.

The interlaminar shear fatigue life of IM7/8551-7 at elevated temperature was also improved by the application of through-thickness compression. A startling observation was that under only a moderate compression of 103 MPa, fatigue failure was eliminated even up to shear stress levels that were 96% of the static strength. These results demonstrate that significant performance gains can be attained with interlaminar compression. With proper design, these gains can be exploited for flywheels and other applications of fiber composite materials.

ACKNOWLEDGEMENTS

The authors gratefully acknowledge the support of the Office of Naval Research, science officer, Dr. Y. Rajapakse, and of the Joint DOE/DoD Technology Development Munitions Program. The contributions by Mr. Will Andrade and Mr. Jeff Petersen to develop the machining techniques and prepare the specimens is also appreciated.

REFERENCES

1. G. C. Pardoen, R. D. Nudenberg and B. E. Wartout, "Achieving Desirable Stress States in Thick Rim Rotating Disks by Variation of Properties," Proc. 1980 Flywheel Technology Symp., 159 October (1980).
2. R. F. Post and S. F. Post, Scientific American, **229**(6), 17 (1973).
3. C. Y. Liu and C. C. Chamis, "Residual Stresses in Filament Wound Laminates and Optimum Programmed Winding Tension," Proc. 20th Annual Meeting of the SPI, Section 5-D, 1 (1965).
4. Hart-Smith, L. J., "Joints" in Engineered Materials Handbook, Volume 1: Composites, ASM International, Metals Park, OH, 1987, pg. 490.
5. Peters, S. T., Humphrey, W. D., and Foral, R. F., "Filament Winding Composite Structure Fabrication," SAMPE, Covina, CA pg. 7-12(1991).
6. Simon, N. J., Drexler, E. S., and Reed, R. P., "Shear/Compression Tests for ITER Magnet Insulation," in Advances in Cryogenic Engineering, Volume 40, Part B, R. P. Reed, et al., Editors, Plenum Press, NY, 1994, pp. 977–983.
7. McManamy, T. J., Kanemoto, G., and Snook, P., "Insulation irradiation test programme for the Compact Ignition Tokamak," Cryogenics, **31** 277–281 (1991).
8. McKenna, G. B., and Mandell, J. F., and McGarry, F. J., "Interlaminar Strength and Toughness of Fiberglass Laminates," 29th Annual Tech. Conf., Reinforced Plastics/Composites Institute, The Society of the Plastics Industry, Washington D. C., Section 13-C, pp. 1–8 (1974).
9. H. T. Hahn and M. N. Kallas, "Failure Criteria for Thick Composites," BRL-CR-691, U.S. Army Ballistic Research Laboratory, Aberdeen Proving Ground, MD, June 1992.
10. C. T. Sun and S. Li, J. Comp. Mater., **22**, 629 (1988).
11. S. W. Tsai amd E. M. Wu, J. Comp. Mater., **5**, 58 (1971).
12. Z. Hashin, J. Appl. Mech., **47**, 329 (1980).
13. R. M. Christensen, J. Eng. Mater. Tech., **120**, 110 (1998).

Table 1. Lamina elastic constants and strengths for IM7/8551-7 (10).

Elastic Constant	Value	Strength	Value
E_{11}	162.0 GPa	X_T	2,417 MPa
E_{22}	8.34 GPa	X_C	1,035 MPa
G_{12}	2.07 GPa	Y_T	73 MPa
G_{23}	2.07 GPa	Y_C	175 MPa
ν_{12}	0.339	S_L	67 MPa(1)
ν_{23}	0.503	S_T	57 MPa

(1) Measured in this study.

Table 2. Predictions for failure of cross-ply or quasi-isotropic laminates of IM7/8551-7 under interlaminar compression.

Failure Theory	Compression Failure Stress (MPa)
Tsai-Wu (1)	183
Tsai-Wu (2)	146
Tsai-Wu (3)	261
Hashin	553
Christensen	392

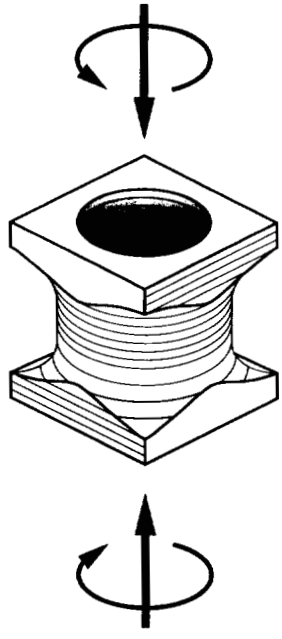

Figure 1. Hollow cylindrical specimen used for combined interlaminar shear and compression tests.

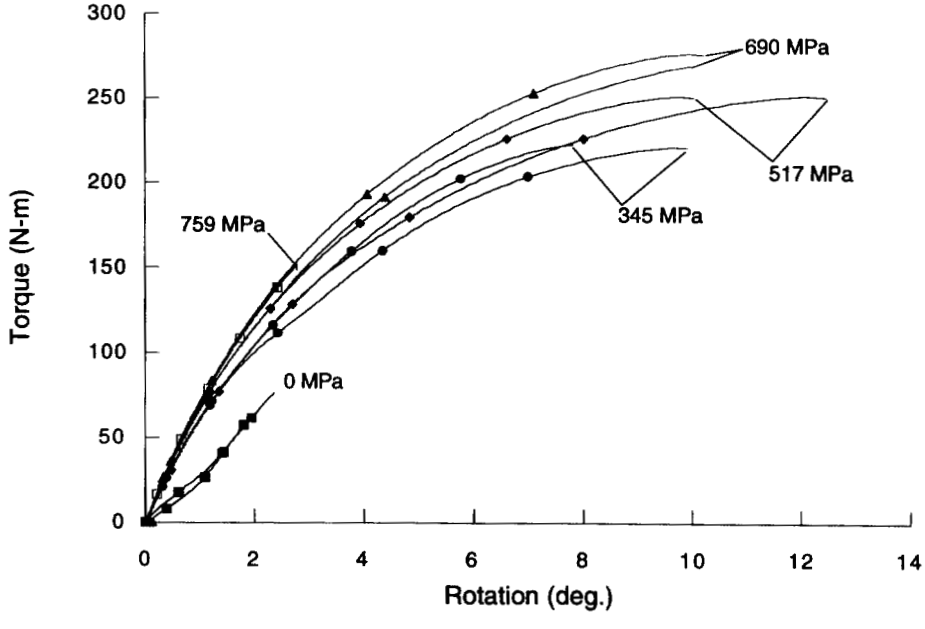

Figure 2. Interlaminar shear response of T300/F584 laminate under levels of interlaminar compression shown.

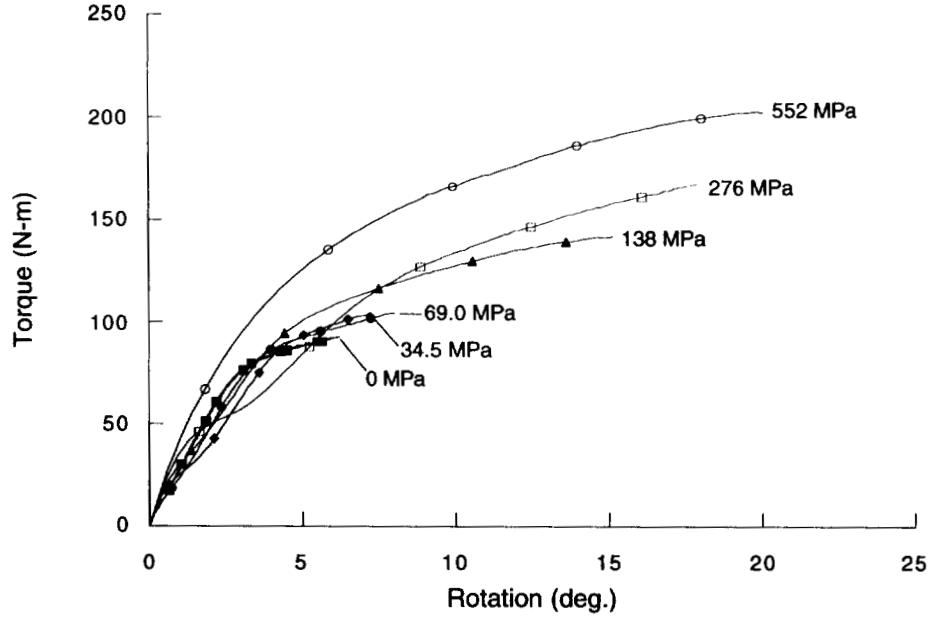

Figure 3. Interlaminar shear response of IM7/8551-7 laminate under levels of interlaminar compression shown.

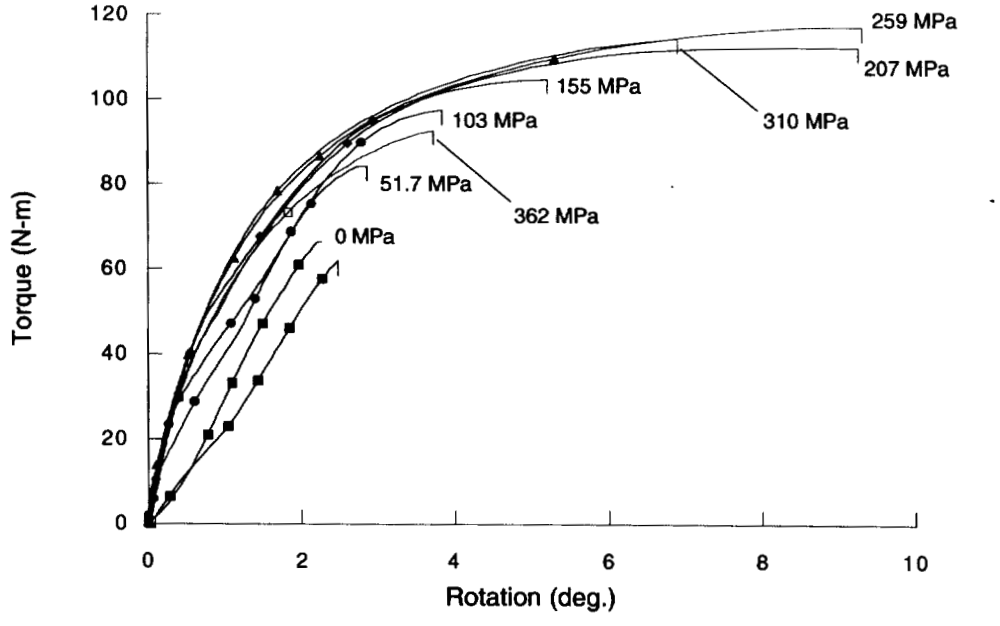

Figure 4. Interlaminar shear response of E-Glass/Vinylester fabric laminate under levels of interlaminar compression shown.

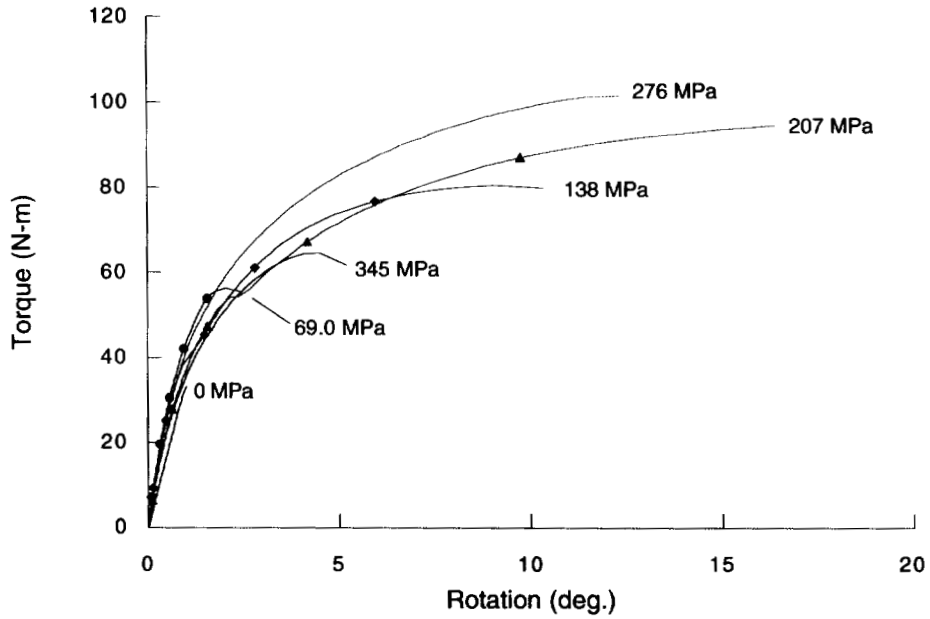

Figure 5. Interlaminar shear response of S2-Glass/epoxy laminate under levels of interlaminar compression shown.

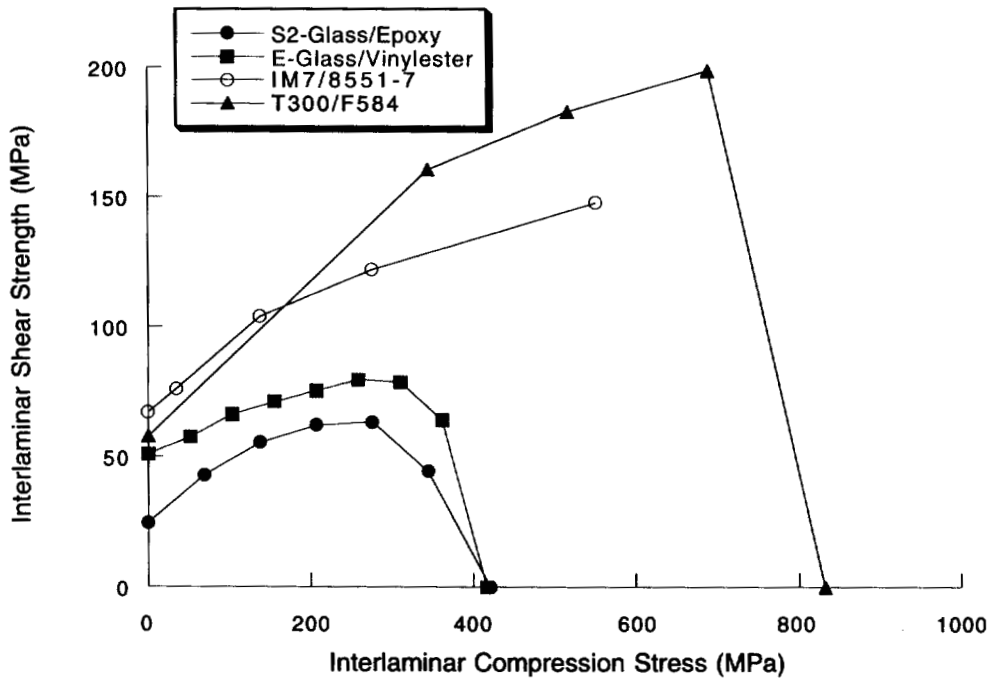

Figure 6. Failure envelope for laminates under combined interlaminar shear and compression stress.

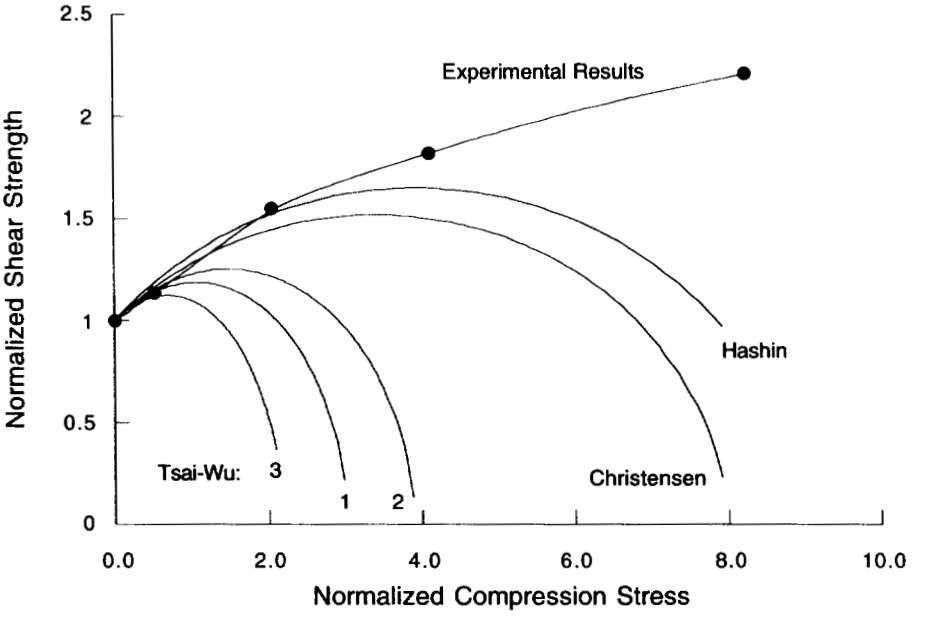

Figure 7. Comparison of predicted and observed failure envelopes for IM7/8551-7 cross-ply laminate under combined interlaminar shear and compression stress.

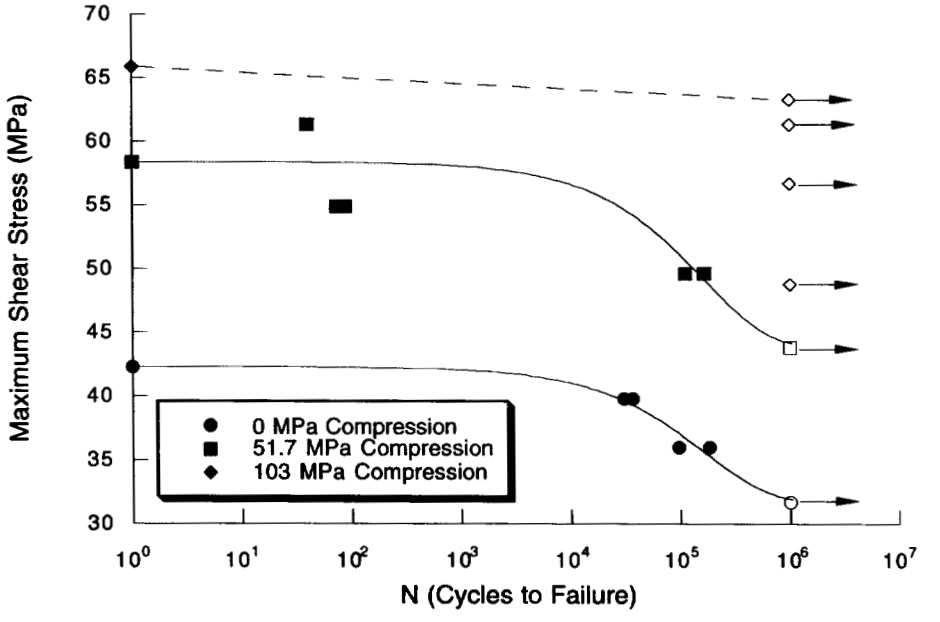

Figure 8. Interlaminar shear fatigue life of IM7/8551-7 at 93°C as a function of interlaminar compression stress.